



Rail fracture monitoring based on ultrasonic-guided wave technology with multivariate coded excitation

Yuan Yang ^{a,*}, Ping Wang ^{a,*}, Yinliang Jia ^a, Lixuan Jing ^a, Yu Shi ^a, Hongwei Sheng ^a, Yi Jiang ^b, Renbao Liu ^a, Yihang Xu ^a, Xin Li ^a

^a College of Automation Engineering, Nanjing University of Aeronautics and Astronautics, Nanjing 210016, China

^b College of Electrical Engineering, Nanjing Vocational University of Technology, Nanjing 210023, China



ARTICLE INFO

Keywords:

Rail fracture
Ultrasonic-guided wave
Coded excitation
Multivariate coding
Pulse compression
Structural health monitoring

ABSTRACT

Steel lay the basis of railroad train traffic. Rail fracture is the most serious injury to the rail, which should be monitored in time. The conventional mono-pulse exciting ultrasonic guide wave (UGW) has low energy, the conventional Barker code has limited coding sequence length and the orthogonal complementary Golay code has the problem of low monitoring efficiency. This study proposes multivariate coded excitation (MCE) to excite UGW to monitor rail fracture, and the feasibility of coding and decoding the method is theoretically derived and verified. Ideally, the MCE generated based on the 3-bit Barker code (B_3 : 1,1, -1) and 4-bit orthogonal complementary Golay code (GA_4 : 1,1,1, -1; GB_4 : 1,1, -1,1) is calculated to have a main-lobe power level (MPL) gain of 8.1020 dB, which is significantly higher than the MPL of Barker and Golay codes. For the proposed method, finite element modeling simulation and experimental study are carried out respectively. Analyze and process the data, and calculate the gain of the difference in amplitude (DIA) between the amplitude of echo caused by rail fracture and the amplitude in the healthy rail. The gain of the DIA of the echoes in the MCE is above 50 dB (experimental data, the value of simulation data is 5 dB) under different degrees of rail fracture, while the gain of the DIA of the echoes caused by the other three excitation methods is below 40 dB (experimental data, the value of simulation data is 1 dB). Simulation and experimental results show that the MCE makes up for the shortcomings of the conventional Barker code and Golay code, improves the excitation energy of the monitoring system, and the high gain of the DIA of the echoes is more conducive to the identification of rail fracture damage.

1. Introduction

The railway has been confirmed as a vital infrastructure. Rail lays a foundation for train operation, and the health of rail takes on critical significance in the safe operation of trains. Rails have a complicated practical use environment, and they remain at the high load state for a long time, thus resulting in the increased probability of rail damage. There are many types of rail damage, including rail crack damage, weld failure, internal nuclear damage, surface peeling, as well as rail fracture [1–4]. To be specific, rail fracture is the most dangerous rail damage. If it is not found and handled in time, it will cause serious accidents (e.g., derailment and rollover of the train) and seriously jeopardize lives and property. At present, the most commonly used rail fracture monitoring methods are primarily dependent on regular inspection by manual and

flaw detection vehicles [5], whereas they still cannot achieve real-time monitoring. Accordingly, the research on the real-time monitoring technology of rail fracture takes on critical significance.

Ultrasonic-guided wave (UGW) monitoring technology has developed rapidly over the past few years. UGW outperforms conventional ultrasonic flaw detection [6] since it exhibits a long propagation distance and high monitoring efficiency [7,8]. However, the multi-modes and dispersion characteristics of this technology will lead to a reduced signal-to-noise ratio and a decreased monitoring distance of the signal. In practical application, an excessively high excitation voltage of an ultrasonic transducer is easy to cause high-voltage sparks, which may endanger the safety of railway lines. Moreover, the energy of the excitation signal can't be further improved due to the limitation of hardware (e.g., the excitation voltage output by the hardware circuit), while the

* Corresponding authors.

E-mail addresses: y.yang20@nuaa.edu.cn (Y. Yang), zeitping@nuaa.edu.cn (P. Wang), jyl@nuaa.edu.cn (Y. Jia), jinglixuan@nuaa.edu.cn (L. Jing), shiyunuaa@nuaa.edu.cn (Y. Shi), zjwx521@sina.com (H. Sheng), 2021101294@niit.edu.cn (Y. Jiang), SX2203012@nuaa.edu.cn (R. Liu), xuyihang@nuaa.edu.cn (Y. Xu), lixin1924@nuaa.edu.cn (X. Li).

monitoring distance and the identification of the rail fracture damage signal are affected. Thus, if the average power is unchanged, the time width of the excitation signal must be increased to obtain higher signal energy, whereas the resolution of damage monitoring will be inevitably reduced [9]. However, coded excitation and pulse compression technology [10] are capable of converting signals from large time-width signals to hour-wide, high-peak signals. In addition, the above techniques use wide-pulse monitoring while maintaining the high damage recognition resolution of narrow pulses [11,12]. In 1979, Takeuchi first applied coding compression technology to medical ultrasound imaging systems [13] and highlighted that the time-bandwidth product of coded signals employed for ultrasound imaging is limited. In 2008, Gran et al. [14] used coded ultrasound (Barker code and Golay code) for the estimation of blood flow velocity to improve imaging accuracy and precision. In 2023, Vienneau et al. [15] addressed the problem of low signal-to-noise ratio and poor imaging performance in transcranial ultrasound imaging detection, and significantly improved image quality by using coded excitation. Coded excitation is more studied and more widely used in medical testing. It is late and less applied in industrial non-destructive testing and structural health monitoring, especially in structural health monitoring of steel rails. Hernandez et al. [16] combined Kasami sequence-coded excitation technology and UGW technology into the rail fracture monitoring system, such that the signal-to-noise ratio and range resolution of the received signals can be improved. In general, coded excitation and pulse compression technologies comprise pulse compression technology based on frequency modulation and pulse compression technology based on phase modulation [17]. Frequency-based coded excitation compression technology has a complex processing process [18]. In rail monitoring, the ultrasonic transducer refers to a piezoelectric transducer with a fixed center frequency, such that the frequency-based coded excitation compression technology is not suitable. The Phase-coded excitation signal is characterized by a large time width, an easy generation of the coded excitation signal, and easy compression of decoded signal, such that it has been extensively employed for non-destructive monitoring [19,20]. Barker coding, Golay orthogonal complementary coding, and other phase coding modes are the extensively used phase coding excitation techniques. Barker code is a type of binary pseudo-random sequence with an ideal aperiodic autocorrelation function [21]. The main lobe and side lobe of the aperiodic autocorrelation function are both isosceles triangles with a base width of 2 T, and the peak value of the main lobe is 13 times that of the side lobe. Malo et al. incorporated Barker code excites UGW into non-destructive monitoring technology, and they significantly enhanced the performance and improved the signal-to-noise ratio of UGW [22]. Although Barker code exhibits good autocorrelation and a low sidelobe level, it only comprises seven types of coding sequences, and the longest sequence length can only reach 13 bits, such that the system performance cannot be further enhanced [23]. The orthogonal complementary Golay code comprises a set of autocorrelated complementary binary sequence pairs A and B [24]. Pulse compression is performed on A and B of the binary sequence respectively, and then vector summing is performed to obtain the final pulse compression result. The ideal pulse compression result with constant main lobe width and no side lobe can be obtained after pulse compression is completed. However, when the orthogonal complementary Golay code is employed for coded excitation and pulse compression, two coding and decoding are required, and the monitoring efficiency declines by 50% [25].

The proposed technology of UGW excited by multivariate coded excitation (MCE) retains the advantages of the two coding methods, so as to overcome the shortcomings of conventional binary coding. The newly generated multivariate coding sequence increases the flexibility of coding sequence length. To be specific, its main-lobe power level (MPL) exceeds those of the Barker code and the orthogonal complementary Golay code, and the monitoring efficiency is double that of the orthogonal complementary Golay code. The MCE excites ultrasonic guided waves for health monitoring of rail fractures, increasing the

energy of the system excitation, which makes the monitoring distance of the system longer and also improves the signal-to-noise ratio of the received signal.

The rest of this study is arranged as follows. In section 2, the process of UGW excited by MCE and pulse compression is theoretically deduced, and the performance evaluation index of UGW excited by coded excitation is proposed. Moreover, the performance index of various coding methods is verified, such that a theoretical basis is laid for subsequent simulation and experimental research. In section 3, the rail model is built in the finite element simulation software, and various excitation signals are compared to excite the UGW to monitor the rail in different states. In section 4, the experimental system and process are introduced in detail, pulse compression processing is performed on the received echo signal, and the gain of signal intensity change attributed to fracture damage is calculated. Section 5 summarizes this study. Lastly, Section 6 is a future work that requires further research and validation.

2. Theory and method

2.1. Multivariate coded excitation and pulse compression method

The developed method of MCE excites UGW and pulse compression can conform to the Barker code and the Golay code and retain the advantages of both codes [9]. The new multivariate coding sequence is recorded as S_3 . Fig. 1 presents the flowchart of coding excitation and pulse compression decoding. The entire process mainly includes modulation of the excitation signal and pulse compression of the received signal. An ultrasonic transducer excites UGWs, which are incident into the rail medium and are used to monitor the rail. Afterward, the ultrasonic transducer receives the signal and compresses it using a pulse compression algorithm. The length of the coding sequence proposed in this study is flexible and theoretically infinite. At the same time, the MPL of MCE is superior to conventional mono-pulse and binary encoding (Barker code and Golay code). In general, the MCE and pulse compression decoding techniques comprise two processes (i.e., excitation signal encoding modulation and receiving signal pulse compression decoding).

2.1.1. Coded excitation

Coded excitation aims to obtain a large time-width excitation signal [26], such that the excitation signal can be endowed with high energy, and the signal's improvement of system monitoring distance and signal-to-noise ratio can be ensured. Fig. 2 shows in detail the process of excitation of UGW signals using multivariate Coded excitation. The generation of multivariate encoding sequences is based on traditional

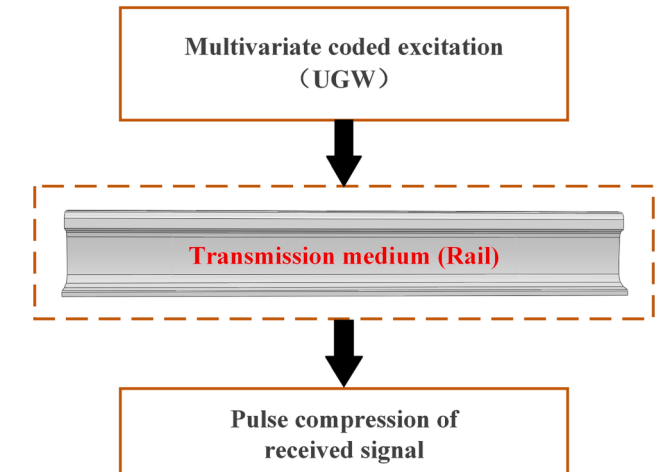


Fig. 1. Schematic diagram of rail monitoring by UGW excited by MCE.

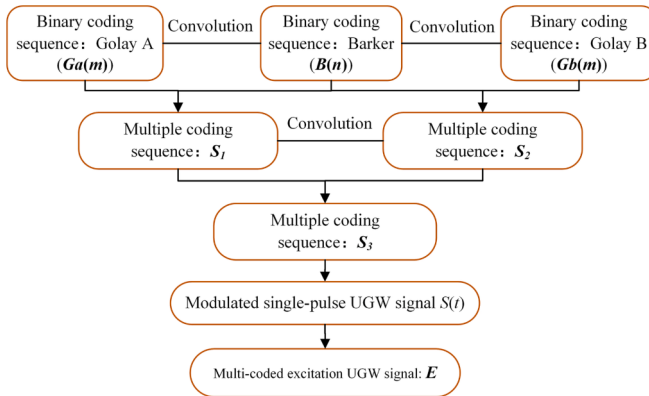


Fig. 2. Schematic diagram of multivariate coding sequence generation.

binary encoding sequences of Barker and Golay codes and is generated through a series of convolutional operations.

The equation for convolution is expressed in Eq. (1) with two sets of sequence variables, $x(n)$ and $h(n)$, where the * sign denotes convolution. When the time permit $n = 0$, the sequence $h(-i)$ is the result of the inversion of the time sequence i of $h(i)$; The inversion of the time sequence makes $h(i)$ flip 180 degrees centered on the longitudinal axis, and this operation of multiplying and then summing is termed convolution.

$$y(n) = \sum_{i=-\infty}^{\infty} x(i)h(n-i) = x(n)*h(n) \quad (1)$$

Among them, the multivariate coded sequence (recorded as S_3) conforms to the Barker code (recorded as B_n) and the orthogonal complementary Golay code (A code recorded as GA_m ; B code recorded as GB_m).

In general, the generation process of the multivariate coded sequence comprises the following processes:

Step 1: First, the orthogonal complementary Golay A code and Golay B code are convolved with Barker code, respectively, and two new multivariate coded sequences are initially determined, expressed as S_1 code sequence and S_2 code sequence, respectively. The convolution operation is written in Eq. (2) and (3).

$$S_1 = GA_m * B_n \quad (2)$$

$$S_2 = GB_m * B_n \quad (3)$$

Where * denotes the symbol of the convolution operation.

Step 2: Following the two new multivariate coding sequences, the convolution operation is performed for the new multivariate coding sequence again, i.e., the proposed multivariate coded sequence S_3 is obtained. The convolution operation is written in Eq. (4).

$$S_3 = S_1 * S_2 \quad (4)$$

Step 3: The newly generated multivariate coding sequence is adapted to modulate the mono-pulse (the mono-pulse refers to the excitation signal of the conventional UGW monitoring rail). The mono-pulse is denoted as $S(t)$, and the waveform after multivariate coding is expressed as E . In this study, the mono-pulse excitation tends to select a narrow bandwidth signal to reduce the effect of the frequency dispersion effect and to reduce the frequency dispersion of UGW in the process of rail propagation [27]. The sinusoidal signal modulated by the Hanning window is selected in this study. The narrow spectrum of the sinusoidal wave modulated by the Hanning window is capable of suppressing the dispersion phenomenon of the UGW, and the sinusoidal wave modulated by the Hanning window with five periods represents the most appropriate excitation waveform [28]. The mono-pulse signal equation is expressed in Eq. (5), and the mono-pulse waveform and its spectrum are

illustrated in Fig. 3 (a) and (b). Furthermore, the excitation signal achieves a frequency of 30 kHz. E is represented as a coded excitation signal, which is formed by convolving the conventional mono-pulse successively by the code elements in the multi-coding sequence S_3 and connecting according to the code element order.

$$S(t) = [1 - \cos(2\pi ft/N_T)][\sin(2\pi ft)] \quad (5)$$

$$E = \{S_3\}^* S(t) \quad (6)$$

Where f is the center frequency of the Hanning window modulated sine wave, N_T is the period number of the sine wave modulated by the Hanning window, t is the duration of the sine wave waveform modulated by the Hanning window, and A is the amplitude of the sine wave modulated by the Hanning window.

In this study, the 3-bit Barker code ($(B_3: 1,1, -1)$) and the 4-bit orthogonal complementary Golay code ($GA_4: 1,1,1, -1$; $GB_4: 1,1, -1,1$) are taken as examples to generate the multivariate code ($S_3: 1,4,4, -2, -5, 0, 5, -2, -4,4, -1$) through the conventional binary coding. Multivariate coding sequence modulates mono-pulse to obtain MCE, denoted as E , the process is shown in Fig. 4(a). Fig. 4(b) shows the spectrum of the MCE signal. As depicted in the spectrum diagram, the center frequency of the MCE signal was still 30 kHz, consistent with the center frequency of the conventional mono-pulse signal.

2.1.2. Pulse compression

After the UGW propagates along the rail, the received signal represents the echo signal with large time width, and the echo signal is recorded as S_e . The relevant equation is expressed in Eq. (6). Among them, it should be noted that UGWs propagate in steel rails with attenuation, and the attenuation function relationship is denoted as $h(x)$ (also known as the transfer function of UGWs in steel rails). Damaged signals are difficult to be distinguished from large time-width signals, such that pulse compression is required for the received signals [29]. In terms of pulse compression, narrow pulse signals are recovered from large time-width signals. Fig. 5. shows in detail the process of receiving signal pulse compression. Pulse compression is based on the initial multivariate sequence and its mirror sequence in the modulation process of encoding sequences, and obtains narrow pulse signals through serial decoding operations.

For the UGW's signal, the pulse compression and decoding process firstly separates the received echo signal through decoding operation, that is, indirectly realizes the excitation effect conversion from the independent Barker code and the orthogonal complementary Golay A code and Golay B code. The specific pulse compression and decoding process is shown in Eq. (7) - (11).

Step 1: Plug Eq. (2) - (6) into Eq. (7). Get Eq. (8).

$$S_e = h(x)^* E \quad (7)$$

$$S_e = h(x)^* \{GA_m * B_n * GB_m * B_n\}^* S(t) \quad (8)$$

Step2: Both sides of Eq. (8) are subjected to the inverse convolution operation with the deconvolution factors ($GB_m * B_n$) and ($GA_m * B_n$), respectively, and Eq. (9) can be obtained:

$$\begin{cases} S_e^{-1}\{GB_m * B_n\} = h(x)^* S(t)^* \{(GA_m * B_n)^*(GB_m * B_n)^{-1}(GB_m * B_n)\} \\ S_e^{-1}\{GA_m * B_n\} = h(x)^* S(t)^* \{(GA_m * B_n)^*(GB_m * B_n)^{-1}(GA_m * B_n)\} \end{cases}$$

$$\Leftrightarrow \begin{cases} S_e^{-1}\{GB_m * B_n\} = h(x)^* S(t)^* \{GA_m * B_n\} \\ S_e^{-1}\{GA_m * B_n\} = h(x)^* S(t)^* \{GB_m * B_n\} \end{cases} \quad (9)$$

Step3: Both sides of Eq. (9) are convolved with ($GA_{-m} * B_{-n}$) and ($GB_{-m} * B_{-n}$), respectively. Among them, where GA_{-m} , GB_{-m} , and B_{-n} are the time reversal sequences of GA_m , GB_m , and B_n , respectively, and Eq. (10) can be obtained:

$$\begin{cases} S_e^{-1}\{GB_m * B_n * GA_{-m} * B_{-n}\} = h(x)^* S(t)^* \{GA_m * B_n * GA_{-m} * B_{-n}\} \\ S_e^{-1}\{GA_m * B_n * GB_{-m} * B_{-n}\} = h(x)^* S(t)^* \{GB_m * B_n * GB_{-m} * B_{-n}\} \end{cases} \quad (10)$$

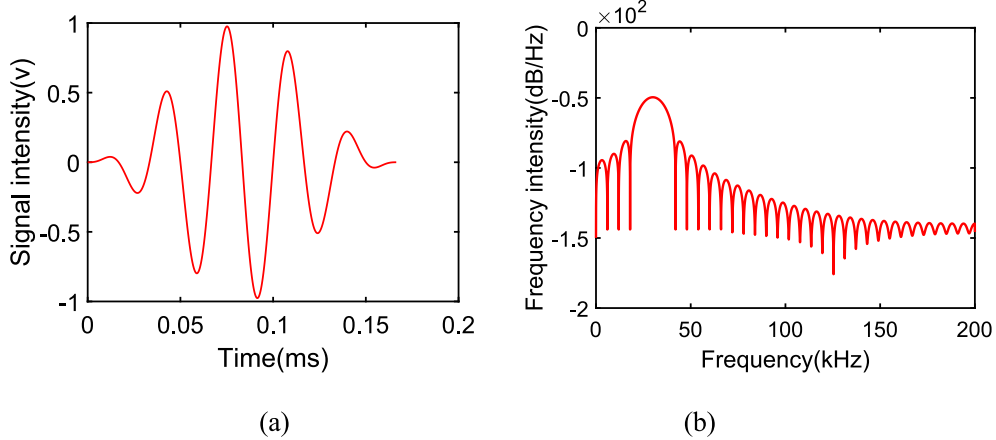


Fig. 3. Hanning window modulated five-period sine function waveform and its Spectrum; (a). Waveform, (b). Spectrum.

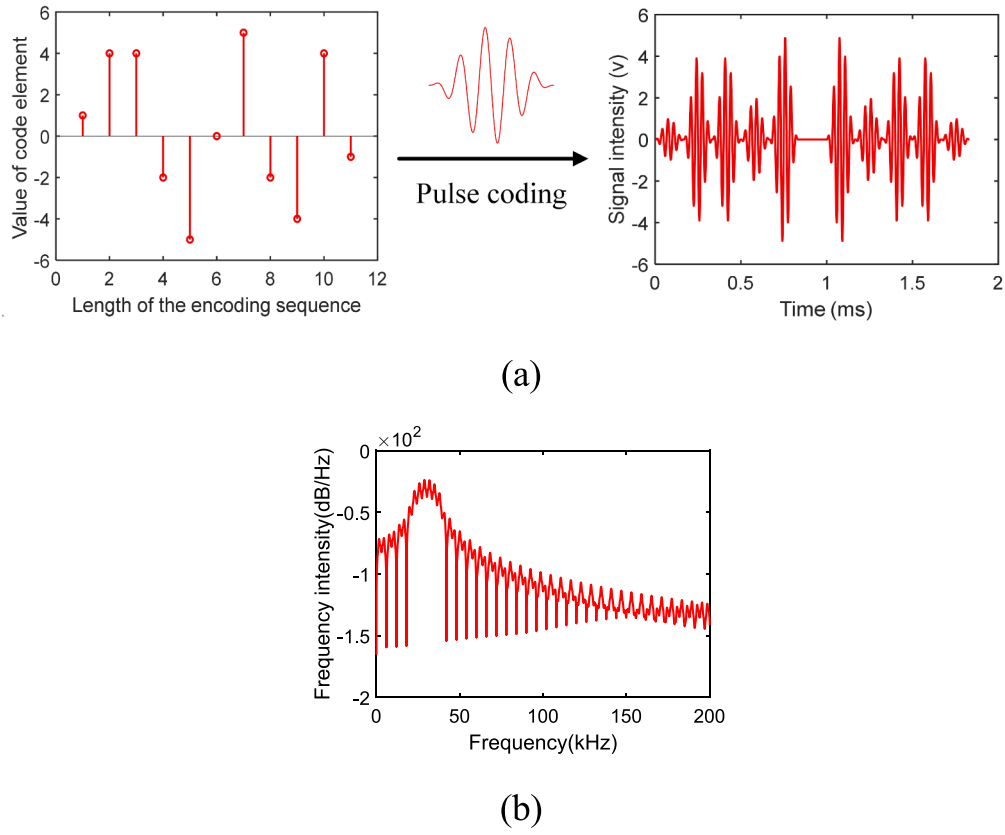


Fig. 4. Schematic diagram of multivariate coding sequence modulated mono-pulse; (a). waveform, (b). spectrum.

Step4: Add the two equation vectors in Eq. (10) to obtain:

$$\begin{aligned} & S_e *^{-1} \{GB_m * B_n * GA_{-m} * B_{-n}\} + S_e *^{-1} \{GA_m * B_n * GB_{-m} * B_{-n}\} \\ & = h(x) * S(t) * \{(GA_m * GA_{-m} + GB_m * GB_{-m}) * (B_n * B_{-n})\} \end{aligned} \quad (11)$$

Where $*$ and $*^{-1}$ represent the convolution and deconvolution operation symbols, respectively. In the equation, $(B_n * B_{-n})$ represents the narrow pulse signal for pulse compression and decoding using the matched filter decoding algorithm adopted by Barker code [19]; $(GA_m * GA_{-m} + GB_m * GB_{-m})$ denotes the pulse compression and decoding narrow pulse waveform signal of the orthogonal complementary Golay A and B codes [24]. Following the above-described equation, the echo signal only covers the transfer function, the mono-pulse excitation signal, and the decoded pulse signal after pulse compression of two basic

binary coded Barker codes, orthogonal complementary Golay A and B codes, while code type correlation noise is not introduced. It is assumed that the rail transfer function $h(x)$ is “1”, such that the most ideal state, the received echo signal is the MCE excitation signal (no loss in the transmission process, the pulse compression results are shown in Fig. 6 (a)). When the UGW propagates in the rail, the amplitude will be attenuated to a certain extent, the frequency will be dispersed and a variety of modes will be generated so that the pulse compression signal will have a tailing (The non-ideal pulse compression results are shown in Fig. 6 (b)). It is discussed here in the most ideal state to more intuitively observe the effect of pulse compression. In this study, 3-bit Barker code (B_3 : 1, 1, -1) and 4-bit Golay code (GA_4 : 1, 1, 1, -1; GB_4 : 1, 1, -1, 1) are serve as the examples.

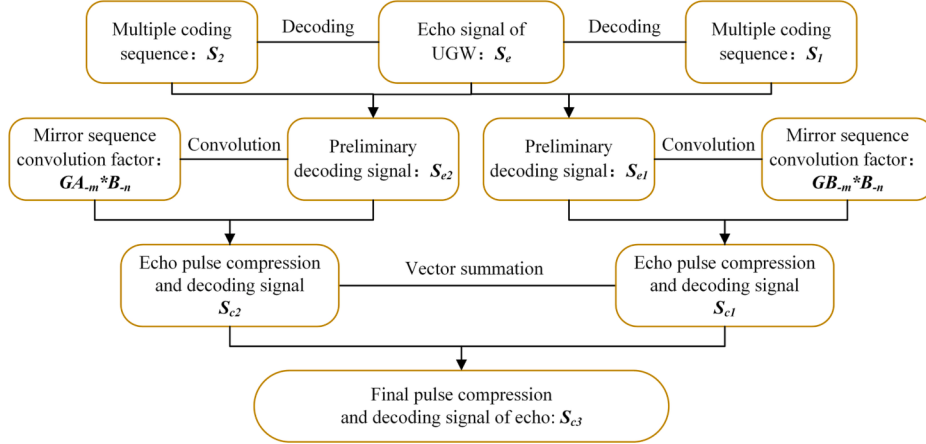


Fig. 5. Schematic diagram of the received signal pulse compression.

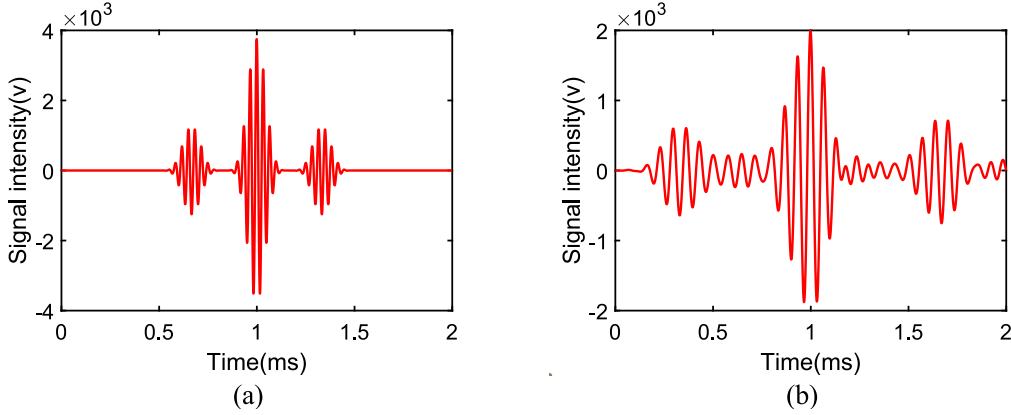


Fig. 6. Final pulse compression and decoding signal; (a). Ideal state, (b). Non-ideal state.

2.2. Performance evaluation of UGW excited by coded excitation

The equation derivation and theoretical analysis of the generation of UGW excited by MCE and the pulse compression of the echo signal are conducted above. Main-lobe power level (MPL)[19,30] is a key index to measure the performance of coded excitation, which is calculated following the peak power and average power of the main lobe. The equation is written in (12).

$$MPL = 10\log_{10}\left(\frac{P_{peak}}{P_{mean}}\right) \quad (12)$$

Where P_{peak} denotes the peak power of the main lobe; P_{mean} is the average power of the decoded signal.

To visually observe the effects of conventional mono-pulse excitation, Barker-coded and Golay-coded excitation, and multivariate coded excitation were proposed in this study. 3-bit Barker code, 4-bit orthogonal complementary Golay code, and the generated multivariate coding sequence as examples. Fig. 7 lists the excitation signal waveform, pulse compression waveform, and the corresponding key indicators. In the above example, it is assumed that the transfer function $h(x)$ is 1 (completely ideal state), such that the MPL is calculated. As indicated by the results, the performance index of MCE is optimal. To be specific, MPL reaches 8.1020 dB.

In practical applications, the received signals are disorderly and mixed with each other, making it difficult to effectively identify and distinguish the main lobe. Therefore, the main lobe power level can't measure the performance of different excitation methods. Referring to the definition of signal-to-noise ratio gain in the literature[19,31], in the

application of rail fracture monitoring in this article, the damage is identified by comparing the gain of the difference in amplitude (DIA) intensity between signals received in different states and signals in healthy states, which in turn can evaluate the performance of various excitation methods. The expression is shown in equation (13).

$$DIA = 20\log_{10}(A_{damage} - A_{healthy}) \quad (13)$$

Where A_{damage} denotes the amplitude of the echo signal caused by rail fracture, and $A_{healthy}$ represents the amplitude of the signal in the healthy condition of the rail.

Fig. 8 presents the MPL calculated under ideal conditions when the mono-pulse waveform $S(t)$ is modulated by the Barker coded, the orthogonal complementary Golay coded, as well as the multivariate coded. To be specific, Barker code selects seven symbols, of which the longest symbol sequence exhibits a length of 13 bits. In theory, the orthogonal complementary Golay code can be infinitely long. In the performance evaluation study, four types of Golay codes with sequence lengths of 2-bit, 4-bit, 8-bit, and 16-bit coding sequences were selected. Fig. 8 illustrates the performance parameters of 16 types of multivariate codes and their basic binary coded modulated mono-pulse. It is noteworthy that the main-lobe power level gain of multivariate coded excitation outperforms those of its underlying binary coded excitation.

The calculation results show that the MPL of the MCE signal are higher than their corresponding conventional binary coding performance, which further shows that the MCE's signal has good performance. As can be seen from Fig. 8, Barker's code reaches the upper limit of 13 bits, which cannot further improve the performance. However, Golay codes can still be further increased, and the performance of

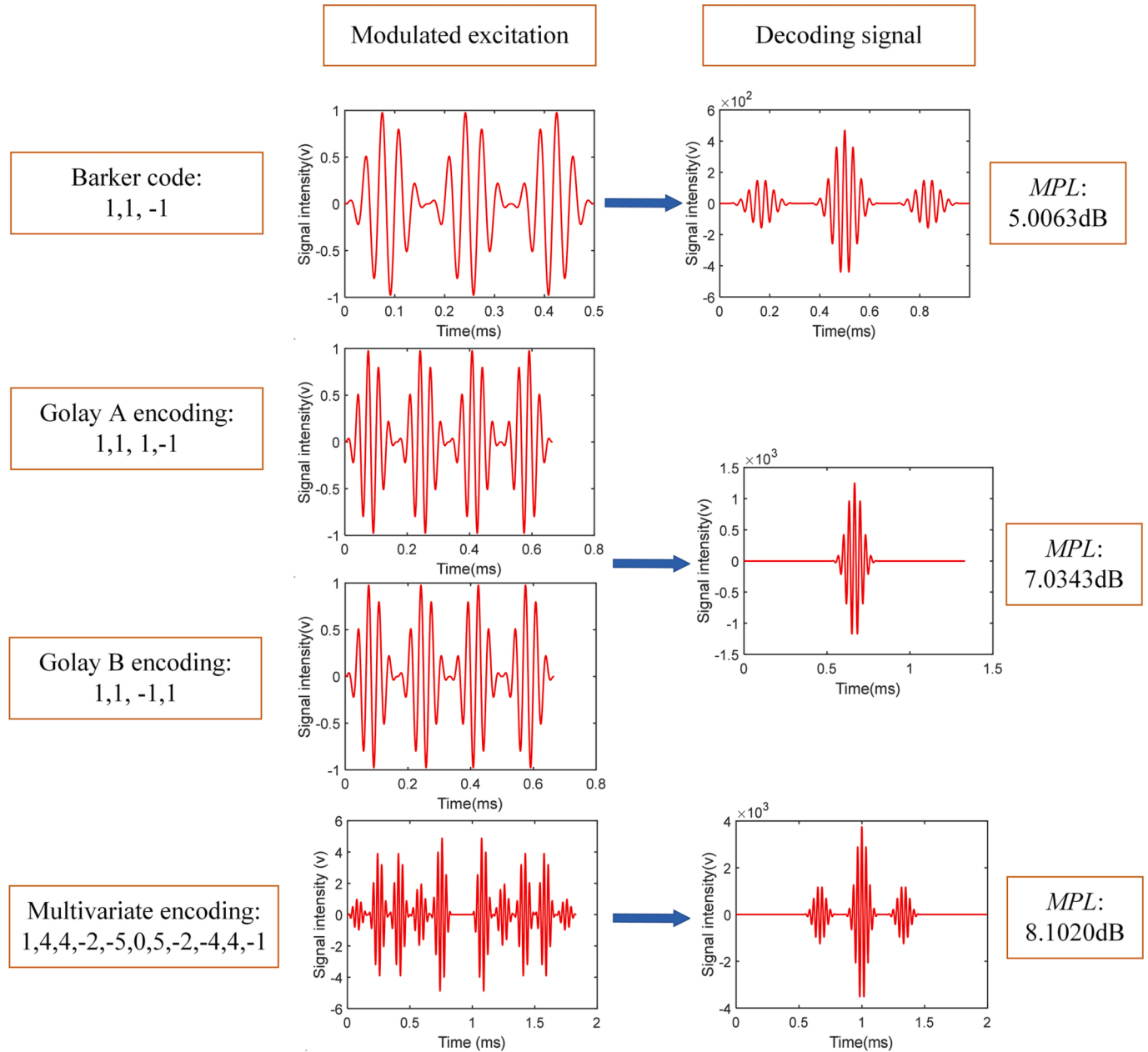


Fig. 7. Excitation signal and pulse compression signal and their corresponding key indicators.

multivariate encoding is also synchronously increasing. Due to the low efficiency of Golay, it requires two encoding and decoding cycles to achieve the final decoding. Overall, as the length of the encoding sequence increases, the excitation performance of multivariate encoding becomes superior.

The above theoretical studies demonstrate the excellent properties of MCE. The following simulation and experimental studies are carried out, the length of the rail model in the simulation study is 10 m (longer distance rail model is too computationally intensive and requires high computer hardware equipment), and the length of the rail in the experiment is 12.5 m (longer distance rails are difficult to obtain). The coded excitations chosen are 3-bit Barker codes and 4-bit Golay codes, as well as multivariate coding sequences generated on their basis. Because the rail is relatively short, it is difficult to verify the encoding of a longer sequence, because when the encoding sequence is longer, the corresponding time-width of the encoded excitation signal is large. In a shorter rail, the starting point of the excitation signal has reached the

end of the rail and is reflected, but the excitation signal is not yet excited, coupled with the interaction of the UGW and various boundaries of the rail, making UGW signal in the entire rail very confusing, which will affect the reception of the ultrasonic guided wave signal.

3. Model and simulation

To verify the propagation characteristics of UGW stimulated by MCE, Barker-coded (B_3 : 1,1, -1), Golay-coded (GA_4 : 1,1,1, -1; GB_4 : 1,1, -1,1) and conventional mono-pulse excited UGW in rail. Abaqus finite element numerical simulation software is used to establish a rail model with a length of 10 m. The rail model is shown in Fig. 9, and the specific parameters of the rail model are listed in Table 1.

Two ultrasonic transducers are arranged at one end of the rail to excite and receive UGW, respectively. The rail is manually cut to simulate rail fracture at a distance of nearly 7.5 m from the ultrasonic transducer. In general, rail fracture arises from rail bottom corrosion

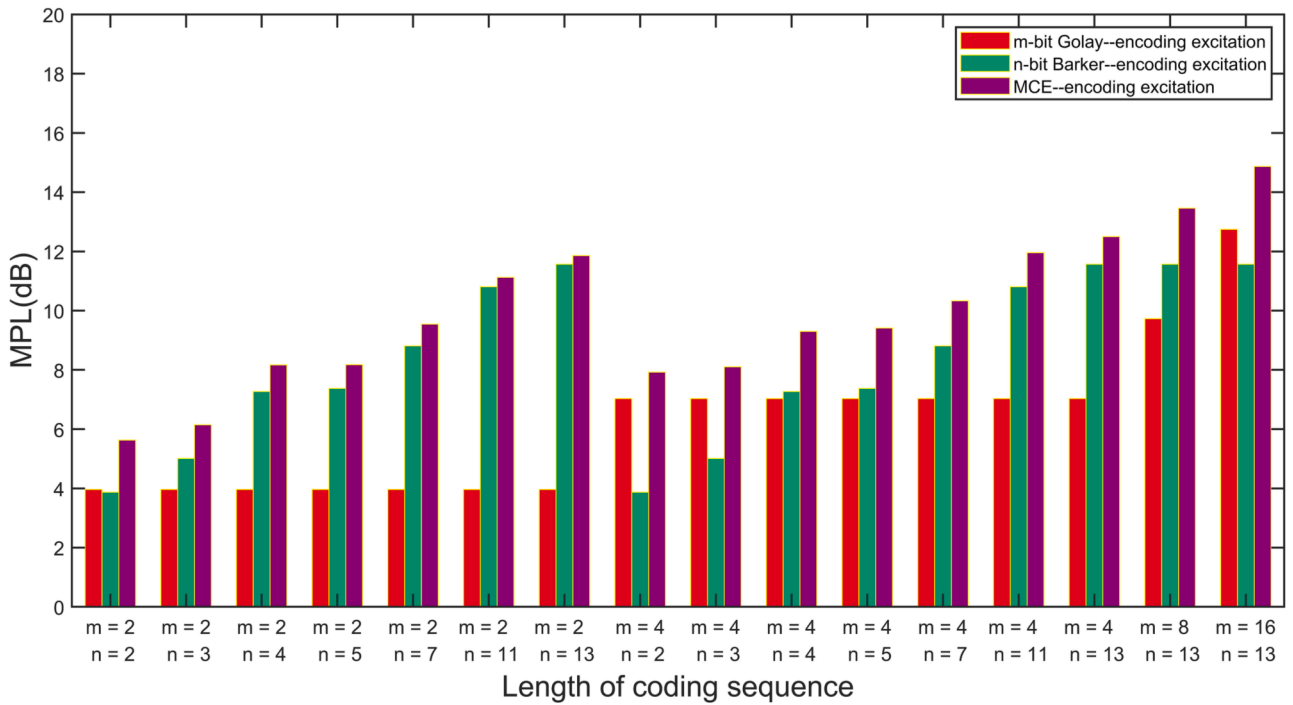


Fig. 8. The MPL gain of mono-pulse modulated by different coding modes.

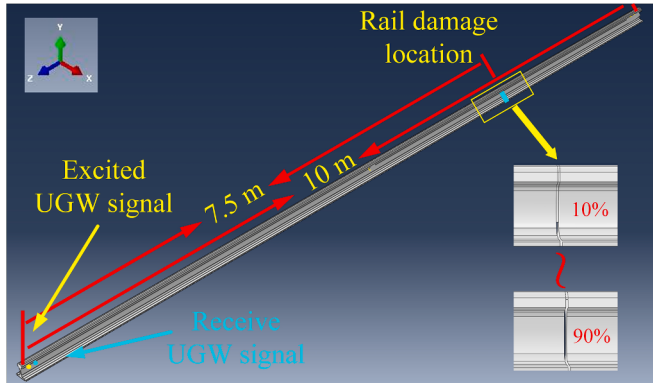


Fig. 9. 3D finite element simulation model of rail monitoring based on UGW technology.

that occurs from the rail bottom to the rail head. Accordingly, when simulating rail fracture manually, cut the rail fracture manually from the rail bottom. The rail fracture depth tends to be deepened from 10% of the rail height as a step (1.75 cm), and the simulated fracture depth accounts for 90% of the rail height (15.75 cm). The degree of fracture of the rail is the percentage of the ratio of the cutting depth to the rail height. There are 10 different rail states from the healthy state of the rail to 90% of the broken state. The excitation signals are conventional mono-pulse excitation, binary excitation, and MCE excitation, respectively. The excitation signals are listed in Fig. 7, and the excitation peak voltage is amplified to 100 V. The cloud image of UGW propagation in the rail is shown in Fig. 10, where (a), (b), and (c) are the rail in a healthy

state, Fig. 10 (a) is the cloud image at 0.1 ms when the UGW is rigorously excited, Fig. 10 (b) is the cloud image at 1 ms, Fig. 10 (c) is the cloud image at 3.2 ms. This time is also about the time taken for the UGW to travel to the 7.5 m damaged site. Fig. 10 (d) to Fig. 10 (h) illustrate the conventional mono-pulse excitation, Golay A code modulated mono-pulse excitation signals, Golay B code modulated mono-pulse excitation signals and multivariate coding modulated mono-pulse excitation signals at 3.2 ms, respectively, indicating the effects of a wide variety of excitation ultrasonic-guided waves in the event of rail fracture.

As depicted in Fig. 10, when the UGW propagates in the rail, the energy of the UGW is gradually attenuated with the increase of the distance. When UGW encounters a fracture, its propagation is blocked, and the echo signal will be generated. As indicated by the comparison of the cloud images in Fig. 10 (d) to Fig. 10 (h), the energy of the excitation signal modulated by multivariate coding sequence (Fig. 10 (h)) is significantly higher than that of the conventional mono-pulse excitation and the binary coded excitation. After a variety of various excitation signals are propagated along the rail, the received echo signals refer to signals with large time width. Fig. 11 lists the received signals and pulse compression signals (with the signals received under the condition of healthy rail as an example). To be specific, matching filtering is performed for conventional mono-pulse signals to further increase the strength of useful signals. Pulse compression is performed on the received large-time-width echo signal, and the echo signal generated by MCE exhibits significantly higher intensity than that generated by the other three excitation signals after pulse compression. In addition, in the process of pulse compression, matched filtering [25] target components with similar waveforms and frequencies to the excitation signal. The noise signal is cluttered and difficult to be compressed, and the intensity of the noise signal isn't significantly enhanced, and the signal-to-noise ratio of the useful signal is further enhanced relatively.

Table 1

Finite element simulation parameters of rail monitoring based on UGW technology.

Rail type	Elastic modulus (Pa)	Poisson's ratio (α)	Density (kg/m^3)	Grid length (m)	Excitation frequency (kHz)
CHN60	2.1e11	0.29	7850	1e-2	30

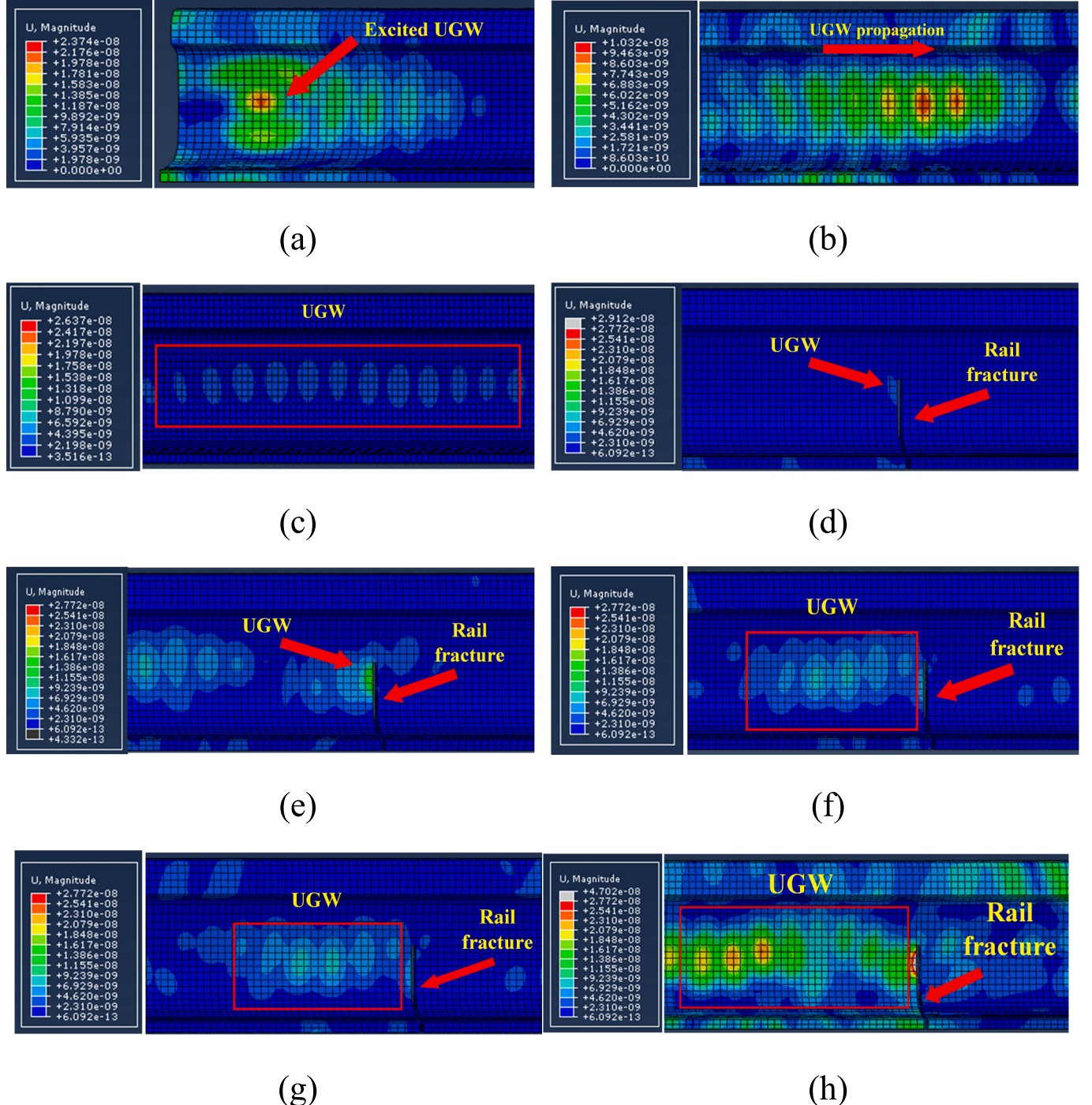


Fig. 10. Propagation cloud image of UGW in rail; (a), (b), and (c) are the cloud images of UGW propagation in healthy rail at 0.1 ms, 1 ms, and 3.2 ms, respectively. (d), (e), (f), (g) and (h) are the signal sources mono-pulse, Golay A coded excitation, Golay B coded excitation, Barker coded excitation and MCE, and the cloud image when the UGW meets the rail fracture, at the time of 3.2 ms.

A total of 10 states ranging from the healthy state of the rail to 90% fracture are set in the numerical simulation. The degree of fracture of the rail is the percentage of the ratio of the cutting depth to the rail height. Given the size of the pictures and the length of the manuscript, the signal diagrams of healthy rail and four types of rail with fracture (fracture depth: 30%, 50%, 70%, 90%) are presented. Figs. 12-15 present the received and pulse compressed and decoded signals. To be specific, Fig. (a) shows the signal diagram at different rail states. The signal that is relatively strong at the beginning refers to the initial wave signal of UGW since the transmitting and receiving of an ultrasonic transducer

are installed together; the receiving probe will receive an initial signal when the excitation probe is excited. Fig. (b) and Fig. (c) are curved surface graphs contributing to the more intuitive distinction of the signal strength of the respective period through the color band. Fig. (c) presents the local signal diagram for avoiding the initial wave. Figs. 12-15 present the signal graphs of conventional mono-pulse excitation, Barker-coded excitation, Golay-coded excitation, and MCE to excite UGW for rail monitoring, respectively.

As depicted by the color band in the figure, when the rail is in a healthy state, the echo time at the 10 m end face of the rail is nearly 8 ms.

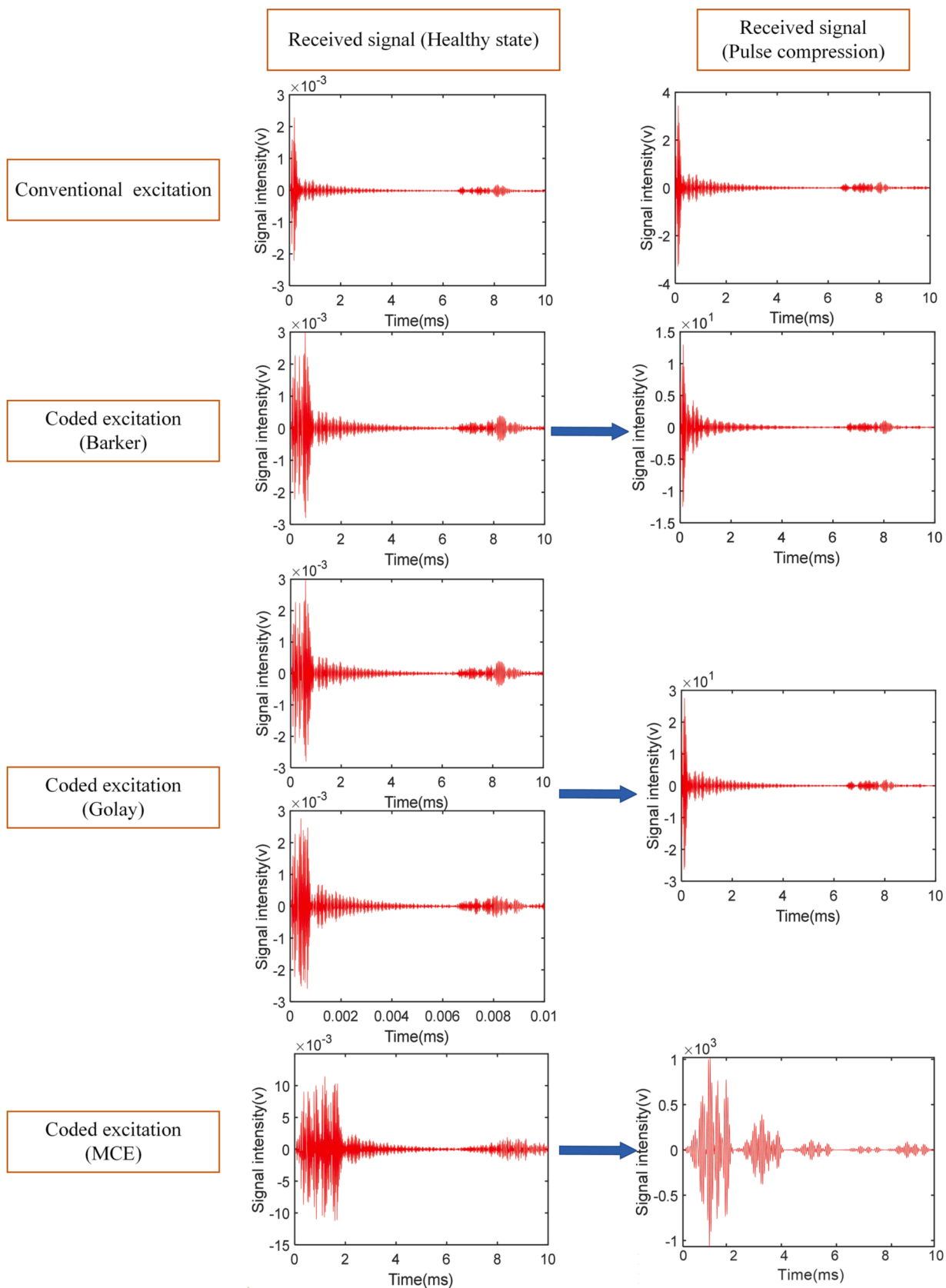


Fig.11. Simulated received signal and its pulse compression signal.

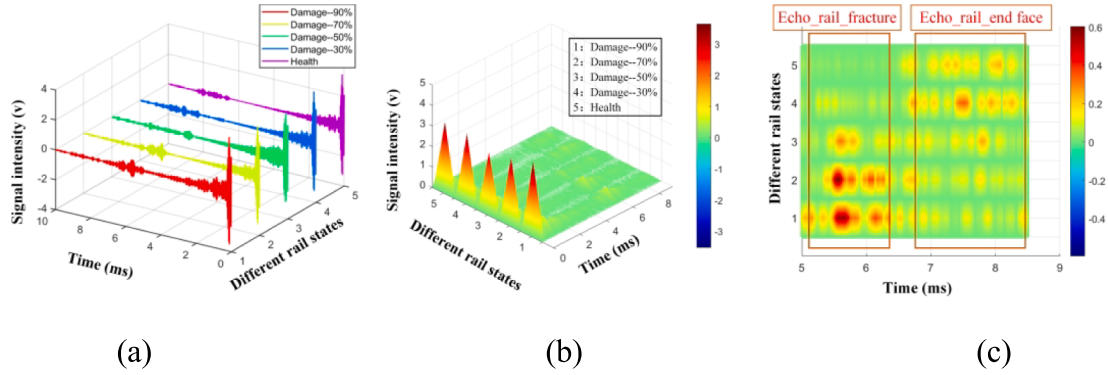


Fig. 12. Conventional mono-pulse excites UGW to monitor rail; (a). Signal maps under different fracture conditions of steel rails;(b) (c). Curved surface graphs from different angles.

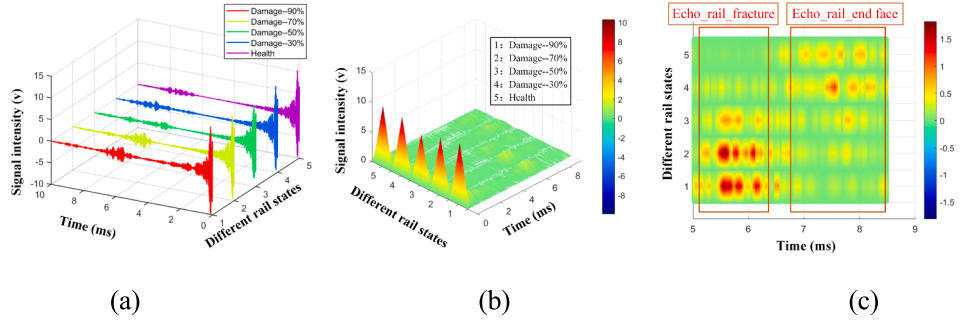


Fig. 13. Barker-coded excitation is used to monitor rail; (a). Signal maps under different fracture conditions of steel rails; (b) (c). Curved surface graphs from different angles.

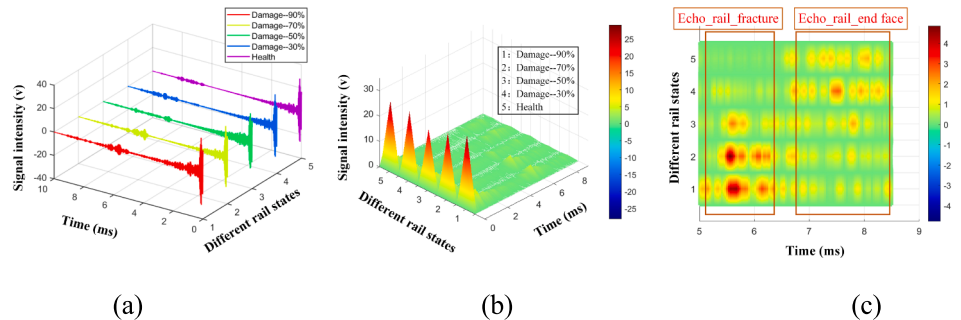


Fig. 14. Golay-coded excitation is used to monitor rail; (a). Signal maps under different fracture conditions of steel rails; (b) (c). Curved surface graphs from different angles.

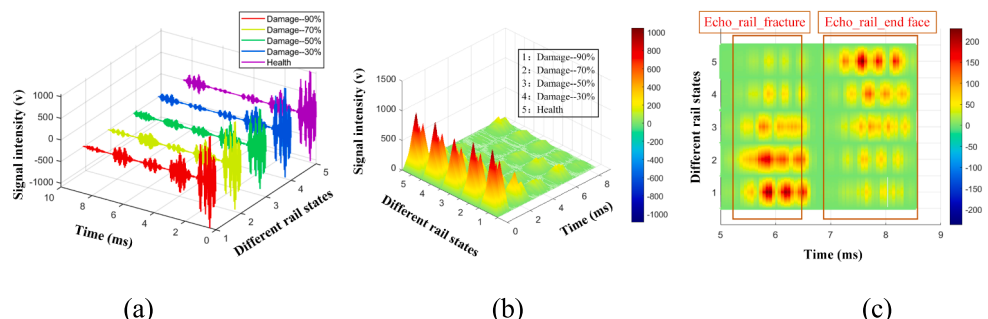


Fig. 15. Monitoring rail by UGW stimulated by MCE; (a). Signal maps under different fracture conditions of steel rails; (b) (c). Curved surface graphs from different angles.

The end face echo signal intensity is reduced with the increase of the rail fracture depth. The corresponding echo time of rail fracture damage at 7.5 m is approximately 6 ms, and the intensity of the rail fracture echo signal is increased as the rail fracture deepens. Four different signals are compared in terms of UGW excitation to monitor rail fracture. The results suggest that the UGW excited by MCE exhibits significantly higher signal intensity than the other three types of excitation signals after pulse compression and decoding, and the signal intensity color band diagram changes more clearly as the rail fracture deepens.

In simulation research, the excitation signals are conventional mono-pulse excitation, Barker-coded excitation, Golay-coded excitation, and MCE. There are a total of 10 states of the rail, ranging from a healthy state to a 90% state of rail fracture. On the established simulation model, finite element simulation is performed for different excitation methods and different rail states. The received signal after pulse decompression is analyzed to extract the echo signal caused by rail fracture damage. Based on Eq. (13), the gain of the difference between the echo signal caused by rail fracture and the signal amplitude in the healthy state is calculated. Under the four excitation modes, the DIA between the echo signal with different rail fracture degrees and the amplitude of the signal under the healthy state is shown in Fig. 16. As depicted in the figure, the DIA of the echo caused by rail fracture is all above 5 dB, whereas the DIA of the echo caused by the other three excitation methods is all below 1 dB. The simulation results show that the multivariate coding excitation is more beneficial to the identification of rail fracture damage.

4. Experiment

4.1. Experimental system and process

An experimental system of UGW monitoring rail is built in a railway maintenance depot base, the three-dimensional system is shown in Fig. 17. To verify the propagation characteristics of UGW excited by MCE, binary coded and conventional mono-pulse in practical rail.

Fig. 7 lists the three excitation waveforms, combined with conventional mono-pulse excitation, resulting in a total of four excitation signals. They are generated by the Waveform Generator (SDG 2082X, Siglent Technologies). The signal generator achieved an initial output voltage of 10 V. Subsequently, the peak excitation voltage is put down to nearly 150 V through the Power amplifier (7602 M, KH/Krohn-Hite), and the sampling rate of the Digital oscilloscope (InfiniiVision DSOX2014A, Keysight) is set to 2.5 M. The experimental rail has a length of nearly 12.5 m, and the distance between the rail fracture and the installation position of the ultrasonic transducer (DYG-C-30-S, Dayu Electronic Technology) is approximately 7 m. The rail is cut by the rail-

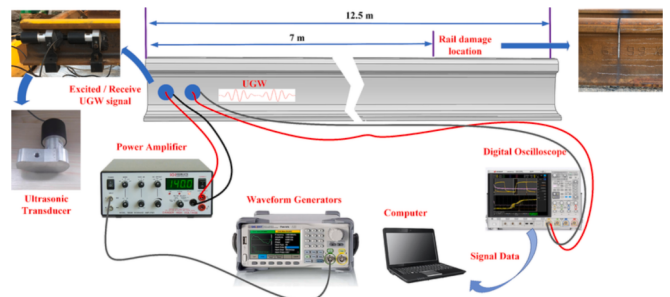


Fig. 17. Diagram of rail fracture monitoring system based on UGW technology.

cutting machine from the top to the bottom, with a respective downward cutting depth of 10% (about 20 mm) of the rail height, till the cutting depth accounts for 90% of the rail height.

5. Experimental data

The pulse compression and decoding process of large time-width echo signal data collected in the experiment is the same as the compression processing of simulation data above. The echo signals received by various excitation signals to monitor the rail are listed in Figs. 18–21, and the signal intensity changes received under different rail states are compared. As indicated by the analysis of the series figures, the echo signal of the end face of the rail appears at nearly 10 ms, and the echo of rail fracture appears at approximately 6 ms. From the healthy state of the rail to the 90% state of rail fracture, the echo signal intensity of the rail end face tends to be decreased, and the echo signal strength arising from rail fracture tends to be increased. The experimental data are consistent with the simulation results, which again shows that the UGW excited by multivariate coding has excellent performance.

To make a more direct comparison between the performance of UGWs stimulated by MCE, conventional mono-pulse, and binary coded, the echo signal arising from rail fracture injury in the experiment was extracted, and the gain of DIA attributed to fracture injury was calculated. The equation for DIA is shown in Eq. (13). The gain of DIA was shown in Fig. 22. In this study, the MCE excitation of UGW for rail monitoring has a signal intensity gain of more than 50 dB at different rail fracture levels, whereas the return signal intensity gain of the other three excitation modes is less than 40 dB.

The above experimental results indicate that the method of MCE proposed in the paper can significantly improve the energy of the excitation signal, and can effectively monitor the rail under different

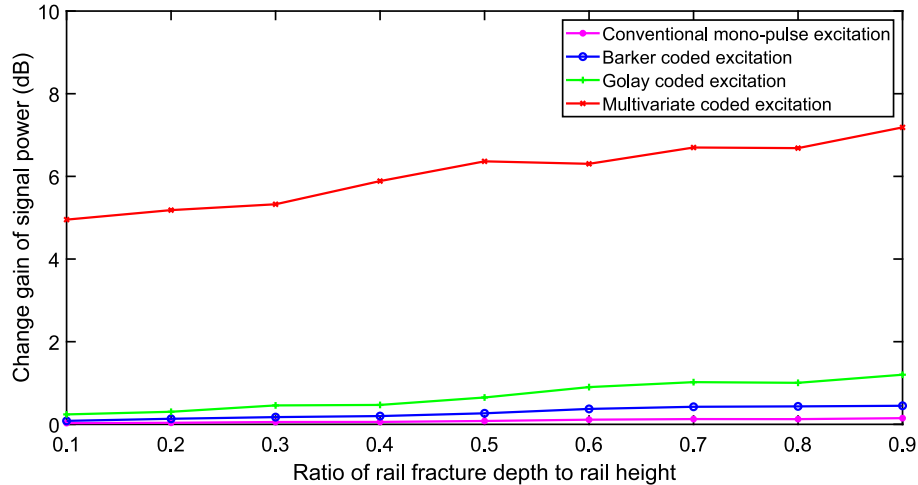


Fig. 16. Signal strength gain varies with the size of rail fracture damage (Simulated data).

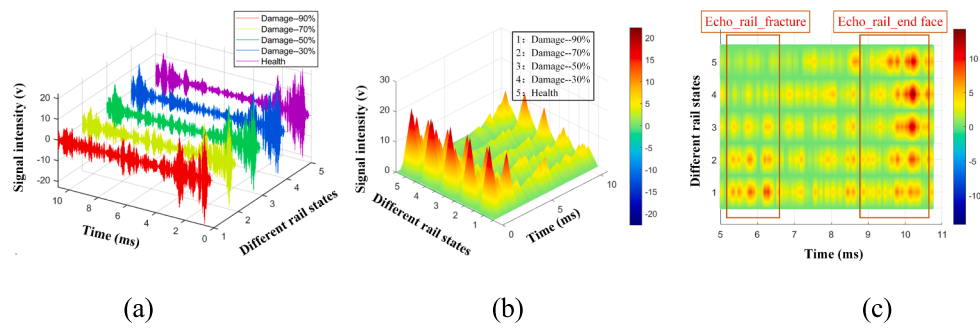


Fig. 18. Conventional mono-pulse excitation is used to monitor rail; (a). Signal maps under different fracture conditions of steel rails; (b) (c). Curved surface graphs from different angles.

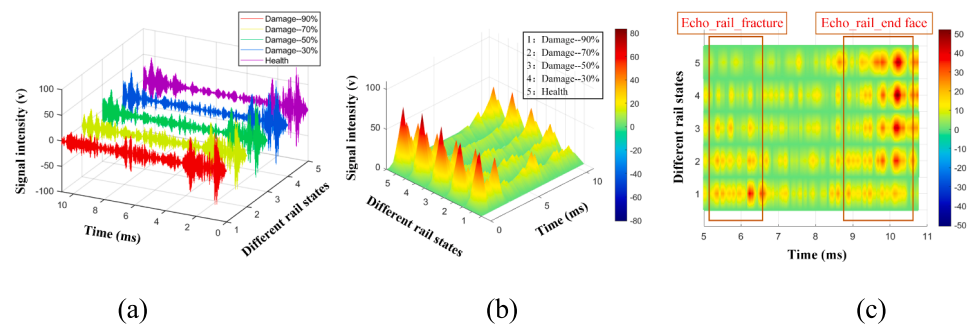


Fig. 19. Barker-coded excitation is used to monitor rail; (a). Signal maps under different fracture conditions of steel rails; (b) (c). Curved surface graphs from different angles.

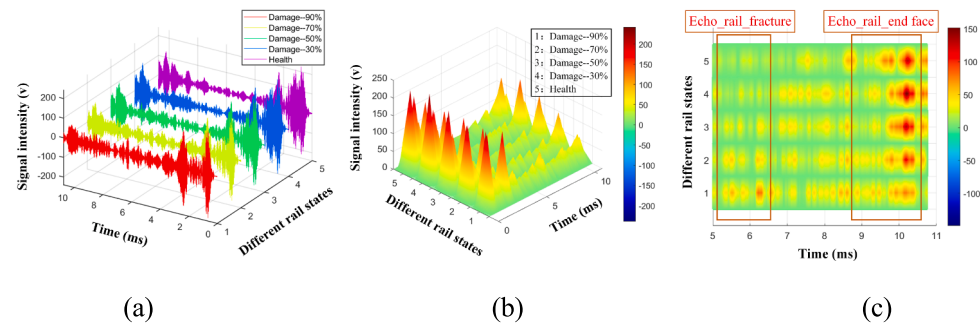


Fig. 20. Golay-coded excitation is used to monitor rail; (a). Signal maps under different fracture conditions of steel rails; (b) (c). Curved surface graphs from different angles.

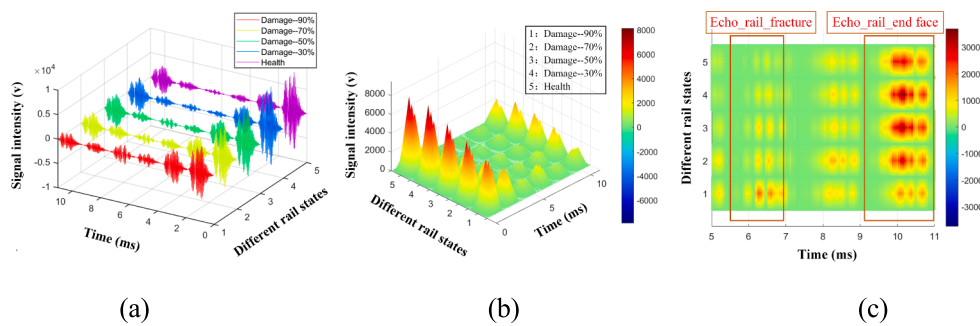


Fig. 21. Monitoring rail by UGW stimulated by MCE; (a). Signal maps under different fracture conditions of steel rails; (b) (c). Curved surface graphs from different angles.

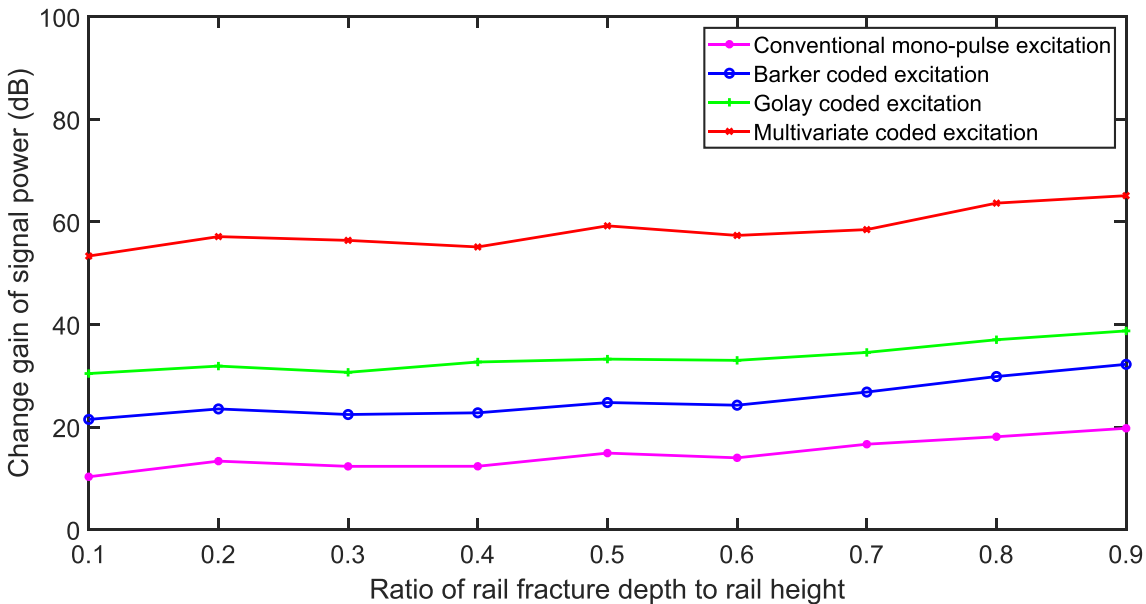


Fig. 22. Signal strength gain varies with the size of rail fracture damage (Experimental data).

fracture states after pulse compression and decoding. Compared with other methods of excitation signal monitoring for steel rails, the gain value of the DIA between different damaged states and healthy states of the steel rails is the largest, which is more conducive to identifying steel rail fracture damage. The experimental results are consistent with the trend of simulation results, which further illustrates the feasibility and excellent of multivariate coded excitation.

6. Conclusion

This study proposes a method of monitoring rail fracture using MCE to excite UGW. First, the multivariate coded excitation and pulse compression process is theoretically deduced. In an ideal case, a multivariate coding sequence generated based on 3-bit Barke codes and 4-bit orthogonal complementary Golay codes is used to modulate conventional mono-pulse as an example. Calculate the MPL of these three types of excitations, and the effect of MCE is the best, reaching 8.102 dB. At the same time, to comprehensively evaluate the performance of encoding excitation, the MPLs of 16 encoding excitation combinations were calculated, and the results showed that the performance of MCE was excellent.

Further, a finite element simulation model for rail fracture monitoring based on the UGW was established. The conventional mono-pulse excitation, binary coded excitation, and multivariate coded excitation are compared as excitation signals to monitor rail fracture damage. After the pulse decompression, the echo signal caused by rail fracture is analyzed and extracted to calculate the DIA of four excitation signals to monitor different degrees of rail fracture. The results show that the performance parameters of UGWs excited by MCE are superior to other excitation methods. The DIA extracted from monitoring rail fracture is higher than 5 dB, while the DIA of the other three monitoring methods is less than 1 dB.

Lastly, the experimental system was built based on the simulation model. The above four excitations were used to excite the UGW, analyze and extract the damaged echo signal, and calculate the DIA of the echo signal of different degrees of rail fracture. The experimental results show that the MCE excites UGW monitoring rail proposed in this study, under different rail fracture levels, the DIA of the echoes is above 50 dB, while the other three excitations of UGWs have the DIA of the other three monitoring methods is less than 40 dB. Moreover, as indicated by the analysis of surface graphs at different rail fracture states, the higher the

fracture degree, the stronger the echo signal intensity arising from the damage will be, and the darker the color of the ribbon will be. The UGW with MCE is proposed to monitor the rail. The curved surface color band diagram exhibits high signal intensity, and the color band change is clear. As revealed by the above-mentioned results, the proposed method applies to the rail fracture monitoring, and the monitoring effect is excellent, consistent with the simulation results.

The proposed multivariate coding sequences enrich the theory and methods of coding and decoding and address the deficiencies of conventional binary coded Barker code and Golay code. The newly proposed MCE exciting UGW monitoring rail is effective in enhancing the signal intensity of rail fracture monitoring using UGW technology. Moreover, this rail can ensure the improvement of the effective distance of rail monitoring, and it takes on critical significance in long-distance rail fracture monitoring.

7. Future work

This study has demonstrated the effectiveness and superiority of MCE for monitoring rail fracture for the first time, whereas some problems still should be investigated in depth. First, matched filtering was selected in this study to achieve compressed decoding of large time-width received signals, and subsequent studies will explore other decoding methods to suppress the sidelobe and further improve the MPL. For instance, the inverse filter in unmatched filtering, Wiener filtering, and other decoding methods. In addition, the theoretical study in Section 2, suggested that the performance of Barker codes cannot be further improved when the sequence length of Barker codes reaches 13 bits, and the multivariate coding method can produce longer sequence lengths. The signal excited by a longer sequence of multivariate encoding has a longer duration and greater energy. In short rail, the UGW has not been fully excited, and the initial UGW has reflected to the excitation point, causing the UGW in the rail to become chaotic and complicated, affecting the reception of the ultrasonic guided wave. Therefore, it is necessary to conduct experimental verification on the rail at hundreds of meters or even longer distances to further verify the performance of the MCE.

Declaration of Competing Interest

The authors declare that they have no known competing financial

interests or personal relationships that could have appeared to influence the work reported in this paper.

Data availability

Data will be made available on request.

References

- [1] D.F. Cannon, K.O. Edel, S.L. Grassie, K. Sawley, Rail defects: an overview, *Fatigue Fract. Eng. Mater. Struct.* 26 (2003) 865–886.
- [2] Y. Li, J. Chen, J. Wang, X. Shi, L. Chen, Study on the effect of residual stresses on fatigue crack initiation in rails, *Int. J. Fatigue* 139 (2020).
- [3] R.P. Gao, M.M. Liu, B. Wang, Y.R. Wang, W. Shao, Influence of Stress Intensity Factor on Rail Fatigue Crack Propagation by Finite Element Method, *Materials* 14 (2021).
- [4] A. Enshaeian, P. Rizzo, Stability of continuous welded rails: A state-of-the-art review of structural modeling and nondestructive evaluation, *Proc. Inst. Mech. Eng. F: J. Rail Rapid Transit.* 235 (2021) 1291–1311.
- [5] M. Micic, L. Brajovic, L. Lazarevic, Z. Popovic, Inspection of RCF rail defects—Review of NDT methods, *Mech. Syst. Sig. Process.* 182 (2023).
- [6] S. Kaewunruen, Discussion of “Field Test Performance of Noncontact Ultrasonic Rail Inspection System” by Stefano Mariani, Thompson Nguyen, Xuan Zhu, and Francesco Lanza di Scalea, *J. Transp. Eng. A: Syst.* 144 (2018).
- [7] J.L. Rose, *Ultrasonic Guided Waves in Solid Media: Plates*, Cambridge University Press, 2014.
- [8] T. Hayashi, W.J. Song, J.L. Rose, Guided wave dispersion curves for a bar with an arbitrary cross-section, a rod and rail example, *Ultrasonics* 41 (2003) 175–183.
- [9] R.Y. Chiao, X. Hao, Coded excitation for diagnostic ultrasound: A system developer’s perspective, in: *IEEE International Ultrasonics Symposium*, Honolulu, HI, 2003, pp. 437–448.
- [10] E. Mozeson, N. Levanon, Multicarrier radar signals with low peak-to-mean envelope power ratio, *Iee Proceedings-Radar Sonar and Navigation* 150 (2003) 71–77.
- [11] B. Lashkari, K.C. Zhang, E. Dovlo, A. Mandelis, Coded excitation waveform engineering for high frame rate synthetic aperture ultrasound imaging, *Ultrasonics* 77 (2017) 121–132.
- [12] H. Elmer, H. Schweinzer, Ieee, High resolution ultrasonic distance measurement in air using coded signals, in: *19th IEEE Instrumentation and Measurement Technology Conference (IMTC/2002)*, Anchorage, Ak, 2002, pp. 1565–1570.
- [13] Y. Takeuchi, An investigation of a spread energy method for medical ultrasound systems. Part one: theory and investigation, *Ultrasonics* 17 (1979) 175–182.
- [14] F. Gran, J. Udesen, M.B. Nielsen, J.A. Jensen, Coded ultrasound for blood flow estimation using subband processing, *IEEE Trans. Ultrason. Ferroelectr. Freq. Control* 55 (2008) 2211–2220.
- [15] E.P. Vienneau, B.C. Byram, A Coded Excitation Framework for High SNR Transcranial Ultrasound Imaging, *IEEE Trans Med Imaging* (2023).
- [16] A. Hernandez, M.C. Perez, J.J. Garcia, A. Jimenez, J.C. Garcia, F. Espinosa, M. Mazo, J. Urena, FPGA-Based Track Circuit for Railways Using Transmission Encoding, *IEEE Trans. Intell. Transp. Syst.* 13 (2012) 437–448.
- [17] T.H. Gan, D.A. Hutchins, D.R. Billson, D.W. Schindel, The use of broadband acoustic transducers and pulse-compression techniques for air-coupled ultrasonic imaging, *Ultrasonics* 39 (2001) 181–194.
- [18] A. Milewski, E. Sedek, S. Gawor, Amplitude weighting of linear frequency modulated chirp signals, *2007 15th IEEE Signal Processing and Communications Applications*, (2007) 1099–1102.
- [19] Z. Fan, X.D. Niu, B.C. Miao, H.Y. Meng, Hybrid Coded Excitation of the Torsional Guided Wave Mode T(0,1) for Oil and Gas Pipeline Inspection, *Appl. Sci.* 12 (2022).
- [20] J.Y. Tang, W.J. Zhu, X.L. Qiu, A.L. Song, Y.X. Xiang, F.Z. Xuan, Non-contact phase coded excitation of ultrasonic Lamb wave for blind hole inspection, *Ultrasonics* 119 (2022).
- [21] J. Lin, J.D. Hua, L. Zeng, Z. Luo, Excitation Waveform Design for Lamb Wave Pulse Compression, *IEEE Trans. Ultrason. Ferroelectr. Freq. Control* 63 (2016) 165–177.
- [22] S. Malo, S. Fateri, M. Livadas, C. Mares, T.H. Gan, Wave Mode Discrimination of Coded Ultrasonic Guided Waves Using Two-Dimensional Compressed Pulse Analysis, *IEEE Trans. Ultrason. Ferroelectr. Freq. Control* 64 (2017) 1092–1101.
- [23] J.M. Howell, Effects of Doppler mismatch on combined Barker codes, *IEEE Trans. Aerosp. Electron. Syst. (USA) AES-6* (1970) 847–851.
- [24] V. Bioglio, I. Land, Polar-Code Construction of Golay Codes, *IEEE Commun. Lett.* 22 (2018) 466–469.
- [25] T. Misaridis, J.A. Jensen, Use of modulated excitation signals in medical ultrasound. Part I: Basic concepts and expected benefits, *IEEE Trans. Ultrason. Ferroelectr. Freq. Control* 52 (2005) 177–191.
- [26] G. Caire, G. Taricco, E. Biglieri, Bit-interleaved coded modulation, *IEEE Trans. Inf. Theory* 44 (1998) 927–946.
- [27] Y. Yang, P. Wang, T.L. Song, Y. Jiang, W.T. Zhou, W.L. Xu, Evaluation of the Transverse Crack Depth of Rail Bottoms Based on the Ultrasonic Guided Waves of Piezoelectric Sensor Arrays, *Sensors* 22 (2022).
- [28] Z. Su, L. Ye, Identification of Damage Using Lamb Waves, in: *Lecture Notes in Applied and Computational Mechanics*, 48, 2009, <https://doi.org/10.1007/978-1-84882-784-4>.
- [29] E.C. Cooke, The early history of pulse compression radar—the history of pulse compression at Sperry Gyroscope Company, *IEEE Trans. Aerosp. Electron. Syst.* 24 (1988) 825–833.
- [30] H.J. Wang, Z. Shi, J.X. He, Compression with considerable sidelobe suppression effect in weather radar, *EURASIP J. Wirel. Commun. Netw.* (2013).
- [31] P. Kim, E. Jung, S. Bae, K. Kim, T.K. Song, Ieee, Barker-sequence-modulated Golay Coded Excitation Technique for Ultrasound Imaging, in: *IEEE International Ultrasonics Symposium (IUS)*, Tours, FRANCE, 2016.